NUMERICAL MODELLING OF ELECTROKINETIC EXTRACTION OF HEAVY METALS FROM HARBOUR SEDIMENTS

M. MASI*, A. CECCARINI**, R. IANNELLI*

** University of Pisa, Department of Energy, Systems, Land and Construction Engineering, Pisa, Italy*

*** University of Pisa, Department of Chemistry and Industrial Chemistry, Pisa, Italy*

Keywords: electrokinetic remediation; dredged sediments; mathematical model; buffer capacity; phreeqc

Abstract. *We implemented a numerical model able to simulate transport of multiple species and geochemical reactions occurring during the remediation of metal-contaminated sediments characterized by a heterogeneous solid matrix, high buffering capacity and aged pollution. The main phenomena described by the model were: (1) chemical species transport through the porous matrix by electromigration and electroosmosis, (2) pH-dependent buffering of H+, (3) adsorption of contaminants onto sediment particle surfaces, (4) aqueous speciation and (5) formation/dissolution of solid precipitates. A constitutive relationship between zeta-potential and pH was used to compute the local electroosmotic permeability. The electroosmotic flow was computed by the volume averaging the electroosmotic permeability. The results of three electrokinetic tests, carried out with different treatment durations (32, 63 and 120 days) were used to validate the model. A good agreement was found between the experimental data and model predictions. In particular, pH and electroosmotic flow were predicted with good accuracy. The predicted metals profiles were also close to experiments profiles for all of the investigated metals (Pb, Zn and Ni) but an overestimation of the removal was observed in the regions close to the anode, possibly due to the significant metal content bound to the residual fraction, quantified with sequential extraction technique. These results encourage the use of the discussed modelling approach as an engineering tool for the design, implementation and removal efficiency prediction of electrokinetic technology at the field scale.*

1. Introduction

Harbour sediments are frequently affected by a wide variety of pollutants. In most cases pollution is caused by the accumulation of contaminants that lasts for decades due to human activities within the harbours or transported from upstream sources.

Remediation of long-term heavy metal contamination is particularly critical, since aging effects cause strong bonds to sediment particles that make pollutant mobilization particularly difficult. Moreover, sediments are often characterized by low-permeability and high acid-neutralizing capacity, due to the high presence of fine particles and carbonates (Peng et al., 2009).

Electrokinetic remediation (EKR) has been successfully employed for the treatment of sediments having these characteristics (Colacicco et al., 2010; Iannelli et al., 2015; Reddy and Cameselle, 2009). This technique relies on the application of a low-intensity electric field to the contaminated mass, which induces the mobilization of contaminants and water through the porous medium toward the electrodes, due to three main transport mechanisms: electromigration (movement of charged ions and molecules), electroosmosis (movement of fluid), and electrophoresis (movement of charged particles). The application of an electric field to the contaminated mass also induces a set of complex effects such as pH changes, electrode reactions and geochemical reactions (Acar and Alshawabkeh, 1993).

Despite many of the abovementioned processes are largely reported in literature and fully understood, their prediction is often a complex task and it is hardly achievable merely on an experimental basis. Especially in the case of sediments with high buffering and sorption capacity, longer remediation times (i.e. months) are required to reach the target clean-up levels. In these cases, an extensive laboratory experimentation would be excessively time-consuming and modelling becomes a necessary tool for the identification of the main parameters affecting the remediation efficiency and for prediction of contaminant extraction. Once the main factors governing the remediation are identified, a mathematical model is also able to provide a way to test different working configurations and remediation schemes for the design and practical implementation of this technology at field scale.

Several models have been proposed to predict electrokinetic extraction of contaminant (Al-Hamdan and Reddy, 2008; Amrate and Akretche, 2005; Choi and Lui, 1995; Paz-García et al., 2011; Yu and Neretnieks, 1996). Most of these models are based on the application of the Nernst-Planck equations to the studied chemical species in the pore fluid solution. These equations are coupled with auxiliary equations in order to guarantee the solution electrical neutrality or with the Poisson equation of electrostatics to calculate the electrical potential locally induced due to the charge unbalance produced when ions are migrating with a different rate.

Many of the developed models show troublesome agreement between the model results and experimental data. This discrepancy can be due to different reasons; generally, it is caused by the high complexity of the mechanisms involved, to the simplifications and assumptions introduced in the model, to strong material heterogeneity or other factors.

The present study aims to address the complicating factors in modelling electrokinetic remediation of real contaminated sediments such as high buffering/sorption capacity and matrix heterogeneity, combining mechanistic and empirical approaches toward the description of these phenomena.

We present a one-dimensional reactive transport model based on the Nernst-Planck equations coupled with a geochemical model. The model describes the contaminant transport driven by chemical and electrical gradients, as well as the effect of surface reactions, speciation of chemical species and their interaction. In the model we consider only the main phenomena which most laboratory investigations recognized as main contributors to the decontamination of saline sediments. The model accounts for: (1) chemical species transport through the porous matrix by electromigration and electroosmosis, (2) induced pH changes, (3) pH-dependent

interaction of H+ and contaminants with sediment particle surfaces, (4) aqueous solution speciation (i.e. formation/dissolution of complexes and solid precipitates) and (5) the interaction between multiple chemical species. The numerical model was validated by comparison with experimental data.

2. Model formulation

In the present study, the electrokinetic remediation processes are divided into transport processes and reactions. The transport of species toward the electrodes mainly occurs by diffusion, electromigration and electroosmosis. Other transport mechanisms not directly related to the application of the electric field may occur (i.e. advective flow due to pressure gradients) but can be neglected, as shown later in the text.

A range of equilibrium and kinetically controlled reactions also occur during electric field application such as electrode reactions, gas-aqueous phase exchange, precipitation/dissolution, adsorption/desorption, complexation, ion exchange, oxidation-reduction, electrochemical deposition. In the present study, we adopt the assumption that chemical reactions are fast enough to reach their chemical equilibrium at each time interval of the numerical integration. A large number of studies adopting this assumption showed reasonable agreement between the model and experimental data (Al-Hamdan and Reddy, 2008; Gomes et al., 2015; Wu et al., 2012).

Under the assumption of local equilibrium, we were able to implement the transport processes and reactions in two separate steps of the numerical integration, using two different software modules. Transport equations were implemented in a finite-element software, which solves the non-linear system of partial differential equations (Nernst-Planck equation) for each of the modelled species. Instead, chemical and geochemical reactions were implemented with the USGS PHREEQC software. The two modules were coupled using a two-step sequential non-iterative split-operator scheme, to calculate transport (first step) and reactions (second step) at each time interval.

Three heavy metals have been investigated in this study (Pb, Zn, Ni). Along with the contaminants, six major species (H^+, OH^-, Na^+, Cl^-, NO_3^-) were also included in the model. A total of sixteen species was implemented, considering the most abundant complexes present in solution under the working conditions (Pb^{2+}, $PbCl^+$, $PbCl_3^-$, $PbCl_4^{2-}$, $PbCl_2$, $PbNO_3^+$, $Pb(NO_3)_2$, Zn^{2+}, $ZnCl^+$, $ZnCl_3^-$, $ZnCl_4^{2-}$, $ZnCl_2$, $ZnNO_3^+$, Ni^{2+}, $NiCl^+$, $NiNO_3^+$).

2.1. Electrokinetic transport

We considered diffusion, electromigration and electroosmosis as the main mechanisms driving the transport of heavy metals. Electrophoretic transport is neglected due to its limited relevance in electrokinetic remediation since the colloid movements are hindered by the immobile phase of the porous medium. Moreover, due to the low hydraulic permeability, it is assumed that the advective flow, i.e. the flow due to pressure gradients, can be neglected because of the lower order of magnitude compared to electroosmotic flow.

Under these assumptions, the flux density per unit cross-sectional area of porous medium J_i (mol m^{-2} s^{-1}) of a dissolved chemical species *i* can be expressed as (Alshawabkeh and Acar, 1992):

$$J_i = -D_i^* \nabla c_i - U_i^* c_i \nabla \phi - k_{eo} c_i \nabla \phi \quad (1)$$

where D_i^* (m^2 s^{-1}) is the effective diffusion coefficient of the i-th specie, c_i (mol m^{-3}) the concentration of the i-th

specie, U_i^* (m^2 s^{-1} V^{-1}) the effective ion mobility, ϕ (V) the electric potential and k_{eo} (m^2 V^{-1} s^{-1}) the coefficient of electroosmotic permeability. Due to the tortuous path followed by the ions in the porous matrix during transport, the effective diffusion and ion mobility coefficients used in Equation 1 take into account the effect of porosity *n* and tortuosity *τ* (Shackelford and Daniel, 1991) and they are defined as:

$$D_i^* = n\tau D_i \tag{2}$$

$$U_i^* = n\tau U_i \tag{3}$$

where D_i (m^2 s^{-1}) and U_i (m^2 s^{-1} V^{-1}) are the diffusion coefficient and ion mobility at infinite dilution, respectively. The value of the tortuosity factor may span in a wide range from 0.01 to 0.84 (Alshawabkeh and Acar, 1992) and the value depends on the specific characteristics of the porous medium.

The diffusivity and ionic mobility can be related to a single property by the Nernst-Townsend-Einstein relation (Alshawabkeh and Acar, 1992):

$$U_i^* = \frac{D_i^* z_i F}{RT} \tag{4}$$

where R (8.314 J K^{-1} mol^{-1}) is the universal gas constant, T (K) the absolute temperature and F (96485 C mol^{-1}) the Faraday's constant.

Applying the law of mass conservation to Equation (1), the mass transport of the *i-th* specie is given by the Nernst-Planck equation:

$$n\frac{\partial c_i}{\partial t} = -\nabla \cdot \left[-D_i^* \nabla c_i - (U_i^* + k_{eo}) c_i \nabla \phi \right] + nR_i \tag{5}$$

where R_i (mol m^{-3} s^{-1}) represents a volumetric net source/sink of c_i due to chemical reactions.

The coefficient of electroosmotic permeability k_{eo} in Equations (1) and (5) is dependent on the zeta potential, which in turn depends upon the characteristics of the porous medium and of the pore fluid. The zeta potential may not be constant in time and space if these characteristics change during the treatment.

Here we adopt a generic exponential relationship, proposed by Eykholt and Daniel (1994):

$$\zeta(mV) = a + b\exp(c \cdot \mathrm{pH}) \tag{6}$$

where *a*,b and *c* are three empirical parameters. These parameters were calibrated from the data collected during the electrokinetic experiments.

The electroosmotic permeability k_{eo} is a space-dependent quantity related to the zeta potential ζ (V), the dielectric constant ε (F m^{-1}) of the fluid and the fluid viscosity η (N s m^{-2}) and it can be expressed as:

$$k_{eo} = -\frac{\varepsilon\zeta}{\eta} n\tau \tag{7}$$

where the minus sign indicates that negatively charged particles produce a direct electroosmotic flow, i.e. from anode to cathode.

Finally, under the assumption that the electric field only varies in the x-direction, we calculated the bulk electroosmotic flow $Q_{eo,x}$ ($m^3\ s^{-1}$) by volume averaging the electroosmotic permeability in the x-direction:

$$\bar{Q}_{eo,x} = -\frac{A\varepsilon}{\eta L} n\tau \int_0^L \zeta E_x \, dx \tag{8}$$

where the quantities outside the integral are assumed constant, L (m) is the specimen length and $E_x = -\partial\phi / \partial x$ (V m^{-1}) is the electric field in the x-direction.

2.2. Chemical reactions

Among the range of reactions that occur when the electric field is applied, we considered: (1) electrolysis of water at the electrodes, (2) pH-dependent adsorption/desorption of H^+ onto the sediment solid matrix, (3) adsorption/desorption of contaminants, (4) aqueous speciation (i.e. formation of complexes), (5) precipitation/dissolution of species.

The first set of electrochemical reactions occur at the electrodes, where water electrolysis takes place:

$$\text{Anode: } 2H_2O \rightleftharpoons O_2(g) + 4H^+ + 4e^- \tag{9}$$

$$\text{Cathode: } 2H_2O + 2e^- \rightleftharpoons H_2(g) + 2OH^- \tag{10}$$

Water oxidation at the anode is included in the model as a boundary condition representing flux of H^+ in the system. Water reduction at the cathode is not considered as a boundary condition, since nitric acid is used at the cathode to neutralize the hydroxyl ions. The flux of NO_3^- is considered instead as a boundary condition for the cathode. We assume in the model that the rate of HNO_3 addition equals the rate of production of OH^- at the cathode and neglected the possible formation of ammonium.

The acid-buffering capacity of the sediments is modelled as a generalized surface complexation reaction. Surface sites are represented by a certain amount of active sites ≡SOH, where S is a metal associated to the solid structure and located at the solid-liquid interface. Depending on the electrolyte pH, these groups are subjected to protonation and deprotonation reactions according to (Stumm and Morgan, 1995):

$$\equiv SOH + H^+ \rightleftharpoons \equiv SOH_2^+ \tag{11}$$

$$\equiv SOH \rightleftharpoons \equiv SO^- + H^+ \tag{12}$$

The equilibrium constants for the above reactions are:

$$K_1 = \frac{[\equiv SOH_2^+]}{[\equiv SOH][H^+]}, \quad K_2 = \frac{[\equiv SO^-][H^+]}{[\equiv SOH]} \tag{13}$$

As a result of this approach, the mass action equations (13) provide a description of the macroscopic dependence of H^+ adsorption as a function of pH but they are not intended to give an accurate representation of

the stoichiometry of the reactions at the molecular scale.

The adsorption of heavy metals (Pb, Ni and Zn) onto the sediment particle surfaces was modelled as an adsorption isotherm with linear distribution coefficient between the liquid and solid phase $K_{d,i}$ (m^3 kg^{-1}), defined as:

$$S_i^a = K_{d,i} c_i \tag{14}$$

where S_i^a (mol kg^{-1}) is the concentration of metal adsorbed onto the solid phase, c_i (mol m^{-3}) is the concentration of the metal in solution.

Surface complexation and adsorption reactions were implemented in PHREEQC. The formation of complexes and precipitates were also calculated by the program. Equations representing these processes are not reported, as they can be found in Parkhurst and Appelo (1999).

2.3. Initial and boundary conditions

The initial and boundary conditions used for the simulations are reported in Table 1. The initial concentrations of all the complexes were set to zero.

Table 1. *Initial and boundary conditions*

Species	Initial concentration (M)	Boundary condition (anode)	Boundary condition (cathode)
H^+	10^{-3}	$J_{H^+} = J / F$	pH = 3
OH^-	10^{-11}	Equilibrium with H^+	pH = 3
Na^+	0.5	$\frac{\partial C_{Na^+}}{\partial t} = 0$	$\frac{\partial C_{Na^+}}{\partial t} = 0$
Cl^-	0.5	$\frac{\partial C_{Cl^-}}{\partial t} = 0$	$\frac{\partial C_{Cl^-}}{\partial t} = 0$
NO_3^-	10^{-3}	$\frac{\partial C_{NO_3^-}}{\partial t} = 0$	$J_{NO_3^-} = J / F$
Pb^{2+}	$4.91 \cdot 10^{-4}$	$C_{Pb} = 0$	$C_{Pb} = 0$
Zn^{2+}	$1.44 \cdot 10^{-2}$	$C_{Zn} = 0$	$C_{Zn} = 0$
Ni^{2+}	$2.59 \cdot 10^{-3}$	$C_{Ni} = 0$	$C_{Ni} = 0$

At the electrodes, the influx of H^+ (at the anode) and of NO_3^- (cathode) were calculated with the Faraday's law of electrolysis $J_i = J / F$, where J_i (mol m^{-2} s^{-1}) is the ion influx and J (A m^{-2}) the current density.

3. Experimental procedure

3.1. Sediment characterization

The sediments were sampled from the Port of Livorno (Italy) from the surface layer of the sea bottom

(approx. 0-50 cm), using a Van Veen-like manual grab sampler. The pH of treated and untreated sediment samples was measured according to ISO 10390:2005. The acid buffering capacity of the sediment was determined by titration method using 0.1 M HCl. Metal content was determined with ICP-OES (after acid digestion in accordance with the US EPA 3050b 1996 and US EPA 7000b 2007 methods). pH and heavy metal content analysis procedures were applied at least to three replicate samples.

3.2. Experimental setup and electrokinetic tests

The setup for electrokinetic tests consisted in an acrylic cell (Figure 1), composed of six parts: the sediment compartment, the electrode compartments, the water and acid reservoirs, the electrolyte solution overflow reservoirs, the power supply and the pH control system. The specimen dimensions were 30x7x7 cm. The anode and cathode were made with a titanium mesh with a Mixed Metal Oxide (MMO). An array of six graphite rod electrodes was placed to monitor the voltage drop across the sediment.

The catholyte was kept at constant pH conditions during the experiments by means of an automated control system. Two pH probes were placed inside the anode and cathode chambers and the measured values were used to automatically control a valve for acid injection into the cathode chamber. Deionized water was added in both electrode chambers at a constant rate in order to compensate the water losses (e.g. electrolysis and evaporation). During the tests, the electroosmotic flow was calculated from mass balance by measuring the volume change in the electrolyte overflows. At the end of each experiment, the material was divided into five locations and analyzed for pH and total metal content. Metal concentrations were also measured in the anolyte and catholyte.

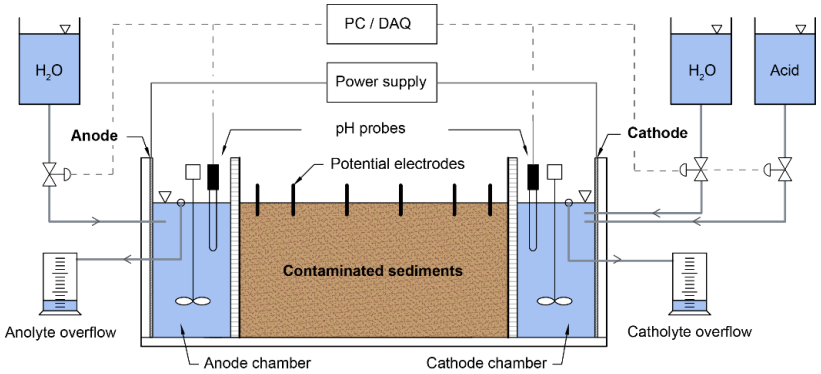

Figure 1. *Diagram of the experimental electrokinetic cell.*

Three experiments (EXP1, EXP2 and EXP3) were carried out applying a constant (DC) current of 40 A/m^2 for 32, 63 and 120 days. Experiment 2 was carried out in our previous work (Iannelli et al., 2015). Nitric acid was added at the cathode to maintain a constant pH of 3. The experimental conditions are summarized in Table 2.

Table 2. *Experimental conditions for the electrokinetic treatments.*

Test	Duration (days)	Applied current density (A/m^2)	Anolyte	Catholyte
EXP1	32	40	Deionized water	HNO_3
EXP2*	63	40	Deionized water	HNO_3
EXP3	120	40	Deionized water	HNO_3

** Experiment results already published in Iannelli et al. (2015).*

4. Results and discussion

4.1. Model parameters

In the numerical model, the reactive-transport of a total of 21 species was set-up. We included in the model only the complexes and solid phases having significant concentration at the working condition (ionic composition and pH), on the basis of preliminary PHREEQC simulations. The selected solid phases included in the model were $Pb_3(OH)_2(CO_3)_2$, $Ni(OH)_2$ and $Zn(OH)_2$.

The values of the diffusion coefficients assigned to each species were taken from literature (Reddy and Cameselle, 2009). Where not available, the complexes were assigned the same diffusion coefficient as their metal constituent. All the equilibrium constants for solution speciation and solid phase reactions were defined as given in the thermodynamic database 'minteq.v4.dat', which is distributed with PHREEQC. The other model parameters were either derived from literature or calibrated through laboratory batch tests and/or with the results of the electrokinetic tests. Table 3 summarizes the parameters adopted in the numerical model.

Table 3. *Model parameters*

Parameter	**Value**	**Unit**	**Description**
τ	0.80	-	Tortuosity factor
n	0.35	-	Sediment porosity
a	69.76	mV	Parameter Eq. 6
b	-20.71	-	Parameter Eq. 6
c	0.15 ± 0.02	-	Parameter Eq. 6
J	40	A/m^2	Applied current density
V_{AN}	8	V	Voltage at the anode
V_{CAT}	0	V	Voltage at the cathode
T	25	°C	Temperature
$\log(K_{d,Pb})$	2.7	-	Pb distribution coeff.
$\log(K_{d,Zn})$	2.4	-	Zn distribution coeff.
$\log(K_{d,Ni})$	2.4	-	Ni distribution coeff.
Reactions	**log(K)**		
$\equiv SOH + H^+ \rightleftharpoons \equiv SOH_2^+$	3.18	-	Protonation reaction
$\equiv SOH \rightleftharpoons \equiv SO^- + H^+$	-7.14	-	Deprotonation reaction

The tortuosity factor was derived from literature. The porosity was experimentally determined. Batch titration tests were carried out to obtain the equilibrium constants of the surface complexation model (Equation 13). The constants K_1 and K_2 were adjusted to fit experimental titration data. The parameters a,b and c of Equation 9 for zeta potential estimation were calibrated minimizing the difference between the electroosmotic flow measured during the experiments and the modelled electroosmotic flow, calculated with Equation 8.

The voltage gradient in the model was set linear and it was assumed constant with time. These strict assumptions were verified during the laboratory experiments which showed that voltage gradient was sufficiently

stable over the entire duration of the tests.

4.2. Numerical simulation results

Figure 2 shows the comparison between the predicted and experimental pH profile. Due to the H^+ produced at the anode, an acid front moves from the anode toward the cathode and progressively acidify the sediment. This process is used to facilitate the desorption of the contaminants from the solid matrix. Overall, a good agreement between the model and the experimental data is observed. The slight disagreement in the region near the anode for the 32 and 63 day experiments might be due both to the constant voltage assumption and to the local equilibrium assumption. Nevertheless, the overall pH values are consistent with the measured values.

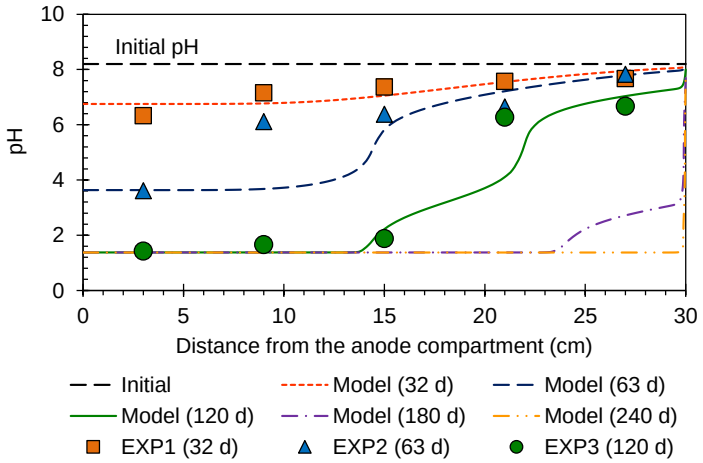

Figure 2. *Predicted and measured pH profiles in the sediment*

The comparison between the electroosmotic flow prediction and electroosmotic flow measured during the experiment with longer duration (EXP3) is presented in Figure 3. The result show a very good agreement between the model and experimental determination. During the experiments, an inversion of the electroosmotic flow direction (from anode to cathode to the opposite direction) was observed after about 30 days of treatment and this change is attributed to the variation of the sediment pH. Along with the change of pH due to the advance of the acid front from the anode, the zeta potential of the sediment particles changed, producing variations in the electroosmotic flow magnitude and direction.

The investigated heavy metals (Pb, Zn and Ni) were either transported by electromigration or by electroosmosis toward the electrodes. The transport of species with higher valence (e.g. Pb^{2+}, Ni^{2+}, $PbCl_4^{2-}$, etc.) was more influenced by electromigration, while the transport of zerovalent complexes occurred only by electroosmosis.

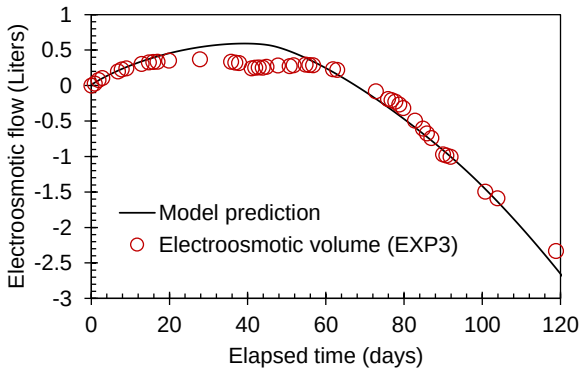

Figure 3. *Comparison between the predicted electroosmotic flow and the volume measured during EXP3*

In Figure 4, the predicted and observed heavy metal profiles are reported as a function of the distance from the anode compartment. The three experimental profiles are very similar, showing a strong dependence from the pH profiles, i.e. where lower pH is observed also lower metal concentration is observed. Small peaks in the concentrations are observed near the cathode, located at about 20 cm from the anodic side due to the accumulation of metals transported toward the cathode and immobilized in the cathodic region due to the higher pH.

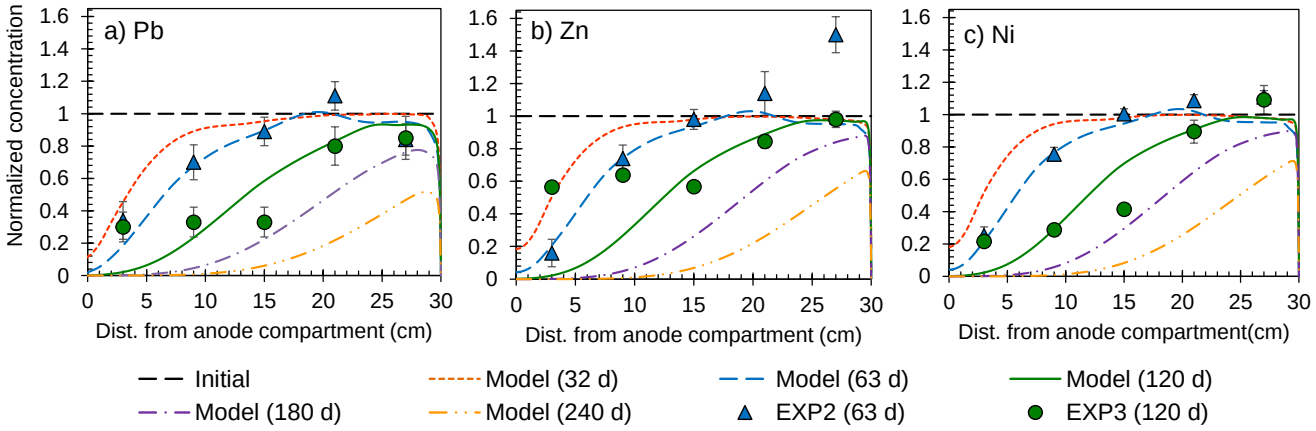

Figure 4. *Model predictions and experimental profiles of Pb, Zn and Ni during electrokinetic remediation. Error bars represent the error measured over three replicate samples*

The simulated profiles are very close for Zn and Ni because both the model parameters defined in Table 1 and the parameters defined in the thermodynamic database were similar. Overall, the profiles are predicted with good accuracy. An overestimation of the removal is observed in the regions close to the anode. This could be due to metal bonding forms in the sediment. With reference to results of the heavy metal speciation in the investigated sediment published in Iannelli et al. (2015), the residual fraction (less mobile fraction) is significant. As a result, the metal concentration in the sediment could hardly be reduced to zero due to higher resilience of this fraction to be affected by the acid front.

In Table 4, the observed and predicted removal percentages are compared. A higher removal is observed for Pb compared to the other metals. This can also be interpreted as a consequence of the lower Pb associated to the residual fraction compared to Zn and Ni. The observed removal rates for Pb are well predicted and it is

estimated that a removal of 85.2% would be achieved applying the treatment for 240 days in the same conditions. The removal of Ni is also well predicted but for Zn an overestimation is observed. This result has been influenced by the high concentration measured near the cathode in the 63-day profile and the apparently inconsistent concentration verified in the section close to the anode in which an increase of Zn is observed in the 120-day profile.

Table 4. *Observed and predicted removal efficiencies (%)*

	EXP2 - 63 days		EXP3 - 120 days		Model prediction
	Observed	Predicted	Observed	Predicted	240 days
Pb	22.3	26.8	47.8	48.4	85.2
Ni	16.0	22.6	41.9	42.2	80.0
Zn	9.5	23.5	28.0	43.9	82.1

5. Conclusions

We implemented a mathematical model which simulates the transport of species and geochemical reactions in a porous matrix under an applied electric field. We applied the model to simulate the electrokinetic extraction of Pb, Ni and Zn from an heterogeneous harbour sediment characterized by high buffering and sorption capacity. The model parameters were calibrated with laboratory batch and bench scale tests. The model runs were compared to the outcome of laboratory electrokinetic tests carried out with different treatment durations (32, 63 and 120 days). The experimental data and model predictions were found to be in good agreement. The predicted pH and electroosmotic flow were very close to observed data. The predicted residual metal concentration in the sediment were also close to experimental profiles for all of the investigated metals but an overestimation of the removal was observed in the regions close to the anode, possibly due to a significant amount of metals bound to the residual fraction. The predicted removal efficiencies were in very good accordance with observed removal percentages for Pb and Ni and moderately overestimated for Zn. These results encourage the use of the model and of the modelling approach as an engineering tool for prediction of remediation efficiency for the design and practical implementation of electrokinetic technology at the field scale. The possibility of using a limited number of investigations or simple tests, e.g. titration, for the determination of the model parameters, is also considered an interesting feature especially for the practical applicability of the model.

References:

[1] Acar, Y.B., Alshawabkeh, A.N., 1993. Principles of electrokinetic remediation. Environ. Sci. Technol. 27, 2638–2647.

[2] Al-Hamdan, A., Reddy, K., 2008. Electrokinetic Remediation Modeling Incorporating Geochemical Effects. J. Geotech. Geoenvironmental Eng. 134, 91–105.

[3] Alshawabkeh, A.N., Acar, Y.B., 1992. Removal of contaminants from soils by electrokinetics: A theoretical treatise. J. Environ. Sci. Heal. . Part A Environ. Sci. Eng. Toxicol. 27, 1835–1861.

[4] Amrate, S., Akretche, D.E., 2005. Modeling EDTA enhanced electrokinetic remediation of lead

contaminated soils. Chemosphere 60, 1376–83.

[5] Choi, Y.S., Lui, R., 1995. A mathematical model for the electrokinetic remediation of contaminated soil. J. Hazard. Mater. 44, 61–75.

[6] Colacicco, A., De Gioannis, G., Muntoni, A., Pettinao, E., Polettini, A., Pomi, R., 2010. Enhanced electrokinetic treatment of marine sediments contaminated by heavy metals and PAHs. Chemosphere 81, 46–56.

[7] Eykholt, G.R., Daniel, D.E., 1994. Impact of System Chemistry on Electroosmosis in Contaminated Soil. J. Geotech. Eng.

[8] Gomes, H.I., Rodríguez-Maroto, J.M., Ribeiro, A.B., Pamukcu, S., Dias-Ferreira, C., 2015. Numerical prediction of diffusion and electric field-induced iron nanoparticle transport. Electrochim. Acta 181, 5–12.

[9] Iannelli, R., Masi, M., Ceccarini, A., Ostuni, M.B., Lageman, R., Muntoni, A., Spiga, D., Polettini, A., Marini, A., Pomi, R., 2015. Electrokinetic remediation of metal-polluted marine sediments: experimental investigation for plant design. Electrochim. Acta 181, 146–159.

[10] Parkhurst, B.D.L., Appelo, C. a J., 1999. User's Guide To PHREEQC (version 2) — a Computer Program for Speciation, Batch-Reaction, One-Dimensional Transport and Inverse Geochemical Calculations, Water-Resources Investigations Report 99-4259.

[11] Paz-García, J.M., Johannesson, B., Ottosen, L.M., Ribeiro, A.B., Rodríguez-Maroto, J.M., 2011. Modeling of electrokinetic processes by finite element integration of the Nernst–Planck–Poisson system of equations. Sep. Purif. Technol. 79, 183–192.

[12] Peng, J.-F., Song, Y.-H., Yuan, P., Cui, X.-Y., Qiu, G.-L., 2009. The remediation of heavy metals contaminated sediment. J. Hazard. Mater. 161, 633–40.

[13] Reddy, K.R., Cameselle, C., 2009. Electrochemical Remediation Technologies for Polluted Soils, Sediments and Groundwater. Wiley.

[14] Shackelford, C., Daniel, D., 1991. Diffusion in Saturated Soil. I: Background. J. Geotech. Eng. 117, 467–484.

[15] Stumm, W., Morgan, J.J., 1995. Aquatic Chemistry: Chemical Equilibria and Rates in Natural Waters, Third edit. ed, Environmental science and technology. Wiley-Interscience.

[16] Wu, M.Z., Reynolds, D.A., Fourie, A., Prommer, H., Thomas, D.G., 2012. Electrokinetic in situ oxidation remediation: assessment of parameter sensitivities and the influence of aquifer heterogeneity on remediation efficiency. J. Contam. Hydrol. 136-137, 72–85.

[17] Yu, J.-W., Neretnieks, I., 1996. Modelling of transport and reaction processes in a porous medium in an electrical field. Chem. Eng. Sci. 51, 4355–4368.